Publications of the Astronomical Society of Japan Advance Access published December 9, 2014

Publ. Astron. Soc. Japan (2014) 00 (0), 1–9
doi: 10.1093/pasj/psu113
Advance Access Publication Date: 2014 0

A long-period eccentric substellar companion to the evolved intermediate-mass star HD 14067

Liang Wang,[1] Bun'ei Sato,[2] Masashi Omiya,[2] Hiroki Harakawa,[2] Yujuan Liu,[1] Nan Song,[1,3] Wei He,[1,3] Xiaoshu Wu,[1,3] Hideyuki Izumiura,[4,5] Eiji Kambe,[4] Yoichi Takeda,[5,6] Michitoshi Yoshida,[7] Yoichi Itoh,[8] Hiroyasu Ando,[6] Eiichiro Kokubo,[6] Shigeru Ida,[2] and Gang Zhao[1,*]

[1]Key Laboratory of Optical Astronomy, National Astronomical Observatories, Chinese Academy of Sciences, 20, Datun Road, Chaoyang District, Beijing 100012, China
[2]Tokyo Institute of Technology, 2-12-1 Ookayama, Meguro-ku, Tokyo 152-8550, Japan
[3]University of Chinese Academy of Sciences, 19A Yuquan Road, Shijingshan District, 100049 Beijing, China
[4]Okayama Astrophysical Observatory, National Astronomical Observatory of Japan, Kamogata-cho, Asakuchi, Okayama 719-0232, Japan
[5]The Graduate University for Advanced Studies, Shonan Village, Hayama, Kanagawa 240-0193, Japan
[6]National Astronomical Observatory of Japan, 2-21-1 Osawa, Mitaka, Tokyo 181-8588, Japan
[7]Hiroshima Astrophysical Science Center, Hiroshima University, 1-3-1 Kagamiyama, Higashi-Hiroshima, Hiroshima 739-8526, Japan
[8]Nishi-Harima Astronomical Observatory, Center for Astronomy, University of Hyogo, 407-2 Nishigaichi, Sayo, Hyogo 679-5313, Japan

*E-mail: gzhao@nao.cas.cn

Received 2014 July 22; Accepted 2014 September 4

Abstract

We report on the detection of a substellar companion orbiting an evolved intermediate-mass ($M_\star = 2.4\,M_\odot$) star HD 14067 (G9 III) using a precise Doppler technique. Either a periodic Keplerian variation with a decreasing linear velocity trend ($P = 1455$ d, $K_1 = 92.2\,\mathrm{m\,s^{-1}}$, $e = 0.533$, and $\dot{\gamma} = -22.4\,\mathrm{m\,s^{-1}\,yr^{-1}}$) or a single Keplerian orbit without linear trend ($P = 2850$ d, $K_1 = 100.1\,\mathrm{m\,s^{-1}}$, and $e = 0.697$) can be well fitted to the radial velocities of this star. The minimum mass ($m_2 \sin i = 7.8\,M_\mathrm{J}$ for the model with a linear trend, or $m_2 \sin i = 9.0\,M_\mathrm{J}$ for the model without a linear trend) suggests a long-period giant planet orbiting an evolved intermediate-mass star. The eccentricity of the orbit is among the highest ones ever detected for planets moving around evolved stars.

Key words: planetary systems — stars: individual (HD 14067) — techniques: radial velocities

1 Introduction

Since the first giant planet orbiting an evolved star was discovered by Frink et al. (2002), progress has been made on the detection and theoretical understanding of planets moving around stars more massive than our Sun in the past decade. Over 90 substellar companions with minimum masses ranging from 0.6 to 40 M_J around giants and subgiants have been detected by precise radial velocity techniques (e.g., Sato et al. 2003; Setiawan et al. 2003; Hatzes et al. 2005; Johnson et al. 2007, 2011;

© The Author 2014. Published by Oxford University Press on behalf of the Astronomical Society of Japan.
All rights reserved. For Permissions, please email: journals.permissions@oup.com

Downloaded from http://pasj.oxfordjournals.org/ at National Astronomical Observatory on January 3, 2015

Sato et al. 2008b; Döllinger et al. 2009; Liu et al. 2009; Wittenmyer et al. 2011; Omiya et al. 2012; Gettel et al. 2012; Lee et al. 2013; Jones et al. 2014), including those in open clusters (e.g., Sato et al. 2007; Lovis & Mayor 2007; Brucalassi et al. 2014) and multiple-planet systems (e.g., Niedzielski et al. 2009; Sato et al. 2013b) and those with masses $\gtrsim 13\,M_{\rm J}$ which thus lie in the brown dwarf regime (e.g., Omiya et al. 2009; Sato et al. 2010; Wang et al. 2012).

Although the number of such companions moving around GK giants is still insufficient to make a statistical study of their physical properties, they are of intense interest because their host stars are the slowly rotating counterparts of intermediate-mass ($1.5 < M_\star/M_\odot < 5$) B–A dwarfs that have evolved off the main sequence, giving us a chance to study planets orbiting stars with masses larger than those of FGK dwarfs. Recent studies have revealed some distinct differences from the FGK main sequence stars. For instance, nearly all detected planets moving around $M_\star > 1.5\,M_\odot$ stars have semimajor axes $\gtrsim 0.6$ au, with only a few exceptions including HD 102956 b (Johnson et al. 2010), HIP 63242 (Jones et al. 2013), WASP-33 b (Collier Cameron et al. 2010), and Kepler-13 Ab (Szabó et al. 2011). Such paucity can be attributed to engulfment by the host stars as they evolved off the main sequence (Sato et al. 2008a; Nordhaus et al. 2010), or the primordial deficiency of short-period planets during their formation (e.g., Currie 2009; Kretke et al. 2009). On the other hand, most planets ever detected around intermediate-mass stars have eccentricities below 0.4. It is natural because most of their hosts are in the post-RGB (core helium burning) phase, and the planetary orbits could have been tidally circularized due to the increasing radii of the host star as it ascends the red giant branch. However, some planets with a high eccentricity ($e > 0.6$) have been discovered (e.g., Sato et al. 2013a; Moutou et al. 2011; Niedzielski et al. 2009), implying the existence of planet–planet scattering scenarios (e.g., Ford & Rasio 2008) or perturbators (e.g., Takeda & Rasio 2005).

In this paper, we report on the detection of a new substellar companion around an intermediate-mass giant HD 14067 from our planet search program using the Subaru 8.2 m telescope, the OAO 1.88 m telescope, and the Xinglong 2.16 m telescope. Observations are described in section 2 and stellar properties are summarized in section 3. Analyses of radial velocities and orbital solutions are given in section 4. In section 5 we give the conclusion.

2 Observations and radial velocity analysis

We have been conducting a precise radial velocity survey for about 300 G–K giants at Okayama Astrophysical Observatory (OAO), Japan, since 2001. To extend this planet search program, we established an international network among Japanese, Korean, and Chinese researchers using three telescopes in the 2 m class in 2005 (East-Asian Planet Search Network: Izumiura 2005), and started the Subaru planet search program in 2006. By taking advantage of the large aperture (8.2 m) of Subaru Telescope, the planet-hosting candidates among a sample of $\sim$300 giants were quickly identified, and the visual magnitudes of $6.5 \leq V \leq 7.0$ enabled them to be subsequently followed up by telescopes in the 2 m class telescopes. For details of the Subaru planet search program, readers are referred to the description in Sato et al. (2010).

We obtained a total of three spectra for HD 14067 in 2007 September, 2008 January, and 2008 August using the High Dispersion Spectrograph (HDS: Noguchi et al. 2002) equipped with the Subaru Telescope. An iodine (I_2) absorption cell was used for providing a fiducial wavelength reference for precise radial velocity measurements (Kambe et al. 2002; Sato et al. 2002). We adopted the setups of StdI2b in the first two runs and StdI2a in the third one, which covered wavelength regions of 3500–6200 Å and 4900–7600 Å, respectively. The slit width was set to 0.″6, giving a resolving power ($\lambda/\Delta\lambda$) of 60000. The typical signal-to-noise ratio (S/N) was 140–200 pixel^{-1} with an exposure time of 30–50 s.

After the observations at the Subaru Telescope, we started follow-up observations using the 1.88 m telescope with the High Dispersion Echelle Spectrograph (HIDES: Izumiura 1999) at OAO. The wavelength region was set to simultaneously cover 3750–7500 Å using the RED cross-disperser with a mosaic of three CCDs. We set the slit width to 200 μm (0.″76), giving a resolving power ($\lambda/\Delta\lambda$) of 67000 with 3.3 pixel sampling, and used an iodine cell for precise wavelength calibration. We collected a total of 27 data points of HD 14067 with HIDES during the period from 2008 October to 2014 January.

In 2012 November we started follow-up observations of HD 14067 with the High Resolution Spectrograph (HRS) attached at the Cassegrain focus of the 2.16 m telescope at Xinglong Observatory, China. The fiber-fed spectrograph is the successor of the Coudé Echelle Spectrograph (CES: Zhao & Li 2001), giving higher wavelength resolution and optical throughput. The single 4 K $\times$ 4 K CCD covers a wavelength region of 3700–9200 Å. The slit width was set to 190 μm, corresponding to a resolving power ($\lambda/\Delta\lambda$) of 45000 with 3.2 pixel sampling. An iodine cell was installed before the fiber entrance to obtain a precise wavelength reference.

The reduction of the echelle spectra was performed by using the IRAF[1] software package in the standard manner.

[1] IRAF is distributed by the National Optical Astronomical Observatory, which is operated by the Association of Universities for Research in Astronomy, Inc., under cooperative agreement with the National Science Foundation.

Downloaded from http://pasj.oxfordjournals.org/ at National Astronomical Observatory on January 3, 2015

The I_2-superposed spectra are modeled based on the algorithm given by Sato et al. (2002, 2012). The stellar template used for radial velocity analysis was extracted by deconvolving an instrumental profile, which was determined from a spectrum of a B-type star taken through the I_2 cell (Sato et al. 2012).

3 Stellar properties

HD 14067 (HIP 10657, BD +23 307, HR 665, TYC 1765-1369-1) is listed in the Hipparcos Catalogue (Perryman et al. 1997) as a G9 III star, with a visual magnitude of $V = 6.53$ and a color index of $B - V = 1.025$. Its Hipparcos parallax $\pi = 6.12 \pm 0.79$ mas (van Leeuwen 2007) corresponds to a distance of 163.4 ± 12.3 pc and an absolute magnitude of $M_V = 0.33$. The effective temperature $T_{\rm eff} = 4815 \pm 100$ K and bolometric correction $BC = -0.329$ were derived from the color index $B - V$ and the estimated metallicity using the empirical calibration of Alonso, Arribas, and Martínez-Roger (1999, 2001). The color excess $E(B - V)$ was calibrated according to the reddening estimation given by Schlegel, Finkbeiner, and Davis (1998), and the interstellar extinction was found to be $A_V = 0.13$. The surface gravity $\log g = 2.61 \pm 0.10$ was determined from the triangular parallax given by the new reduction of the Hipparcos Catalogue (van Leeuwen 2007). The iron abundance [Fe/H] was determined from the equivalent widths of ~ 30 unblended Fe lines measured from an iodine-free stellar spectrum taken with HIDES, and the LTE model atmosphere adopted in this work were interpolated from the ODFNEW grid of ATLAS9 (Castelli & Kurucz 2004). The stellar mass, radius, and age were estimated by using a Bayesian approach similar to that of da Silva et al. (2006). We used the Geneva database (Lejeune & Schaerer 2001), which covers the phases from the main sequence to the early asymptotic giant branch (EAGB) stages for stars with $2 \leq M_\star/M_\odot \leq 5$, to interpolate an extensive grid of stellar evolutionary tracks, with $\Delta M = 0.05$ within $1.2 \leq M_\star/M_\odot \leq 3.6$, Δ[Fe/H] $= 0.02$ within $-0.4 \leq$ [Fe/H] $\leq +0.3$, and 500 interpolated points in each track, spanning the whole evolutionary history. For each data point, the likelihood functions of $\log L$, $T_{\rm eff}$, and [Fe/H] were calculated to match the observed values by assuming a Gaussian error for each parameter. To simplify the calculation, we adopted uniform prior probabilities of mass and [Fe/H], but weighted the probability of each model with its spanning age along its evolutionary track. The details of the method will be described in an upcoming paper (L. Wang et al. in preparation). The probability distribution functions (PDFs) of the parameters yield $M_\odot = 2.4 \pm 0.2\ M_\odot$, $R = 12.4 \pm 1.1\ R_\odot$, and age $= 0.69 \pm 0.20$ Gyr, and the probability that after the passage through the RGB tip the star is in core helium burning phase is $\sim 97\%$. In figure 1, we plotted the HD 14067 on an H–R diagram, together with the evolutionary tracks from Lejeune and Scharer (2001) of stars with different masses and metal contents. The macroturbulence velocity was estimated from the empirical relations of Hekker and Meléndez (2007), and the stellar rotational velocity $v \sin i$ is less than $1\ {\rm km\,s^{-1}}$ according to de Medeiros and Mayor (1999). We also determined the lithium abundance by fitting the line profile of Li I λ6707.8 Å doublet using the spectra synthesis method with the IDL/SIU package. The results of $\log A({\rm Li})_{\rm LTE} = 0.53$ and $\log A({\rm Li})_{\rm NLTE} = 0.73$ suggest HD 14067 is an Li-depleted giant (Liu et al. 2014). The derived stellar parameters of HD 14067 are listed in table 1. Furthermore, the star shows no significant emission in the core of Ca II HK lines, as shown in figure 2, which suggests that HD 14067 is chromospherically inactive.

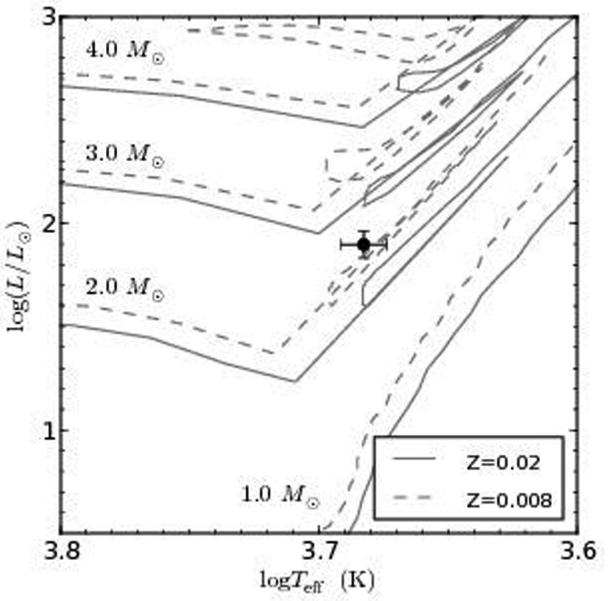

Fig. 1. H–R diagram. The filled circle represents HD 14067, with the errorbars corresponding to the uncertainties given in table 1. The solid and dashed lines represent the evolution tracks from Lejeune and Scharer (2001) for stars of $M = 1 \sim 4\ M_\odot$ with $Z = 0.02$ (solar metallicity) and $Z = 0.008$, respectively.

4 Radial velocities and orbital solutions

We obtained a total of 52 velocity data points (27 from OAO, 22 from Xinglong, and 3 from Subaru) of HD 14067 over a span of more than 5 yr. The radial velocities (RV) are listed in table 2 together with their estimated uncertainties. The generalized Lomb–Scargle periodogram (Zechmeister & Kürster 2009) of HD 14067 shows a significant peak with *FAP* (false-alarm probability) $< 1 \times 10^{-6}$

Downloaded from http://pasj.oxfordjournals.org/ at National Astronomical Observatory on January 3, 2015

Table 1. Stellar parameters of HD 14067.

Parameter	HD 14067
Spectral type	G9 III
π (mas)	6.12 ± 0.46
Distance (pc)	163.4 ± 12.3
V	6.53
$B-V$	1.025
A_V	0.14
M_V	0.33
BC	-0.329
$T_{\rm eff}$ (K)	4815 ± 100
$\log g$	2.61 ± 0.10
[Fe/H]	-0.10 ± 0.08
$v_{\rm t}$ (km s^{-1})	1.30 ± 0.15
L ($L_\odot$)	79 ± 12
R ($R_\odot$)	12.4 ± 1.1
$M_\star$ ($M_\odot$)	2.4 ± 0.2
age (Gyr)	0.69 ± 0.20
$v_{\rm macro}$ (km s^{-1})	5.44 ± 0.45
$v \sin i$ (km s^{-1})	< 1 (de Medeiros & Mayor 1999)
log A(Li)	0.53 (LTE), 0.73 (NLTE)

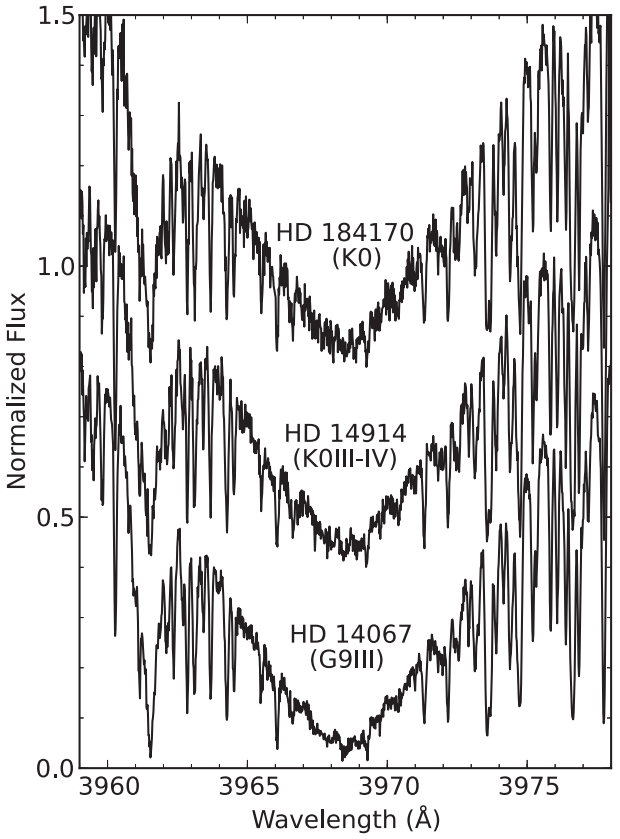

Fig. 2. Spectra in the region of Ca H lines. Stars with a similar spectral type to HD 14067 are also shown in this figure. A vertical offset of 0.4 is added to each spectrum.

Table 2. Radial velocities of HD 14067.

JD (−2450000)	Radial velocity (m s^{-1})	Uncertainty (m s^{-1})	Observatory
4758.11638	33.7	3.2	OAO
4796.20144	51.3	3.3	OAO
4820.01616	41.8	3.0	OAO
5164.16162	104.3	3.5	OAO
5444.14944	106.1	3.2	OAO
5525.16330	113.6	3.2	OAO
5545.11627	106.2	4.0	OAO
5580.00227	100.2	5.7	OAO
5612.94961	116.7	4.5	OAO
5628.91329	87.9	3.8	OAO
5786.27403	− 3.9	3.5	OAO
5811.19593	− 15.1	3.9	OAO
5853.23042	− 94.8	5.1	OAO
5854.22657	− 88.9	3.5	OAO
5879.18379	− 109.5	3.8	OAO
5922.00916	− 81.2	3.8	OAO
5938.00117	− 76.6	3.8	OAO
5976.91135	− 79.0	3.5	OAO
6139.23229	− 44.8	4.5	OAO
6157.28469	− 37.3	3.8	OAO
6212.29616	− 53.1	3.8	OAO
6235.19638	− 63.7	4.4	OAO
6250.20981	− 25.0	3.6	OAO
6284.05633	− 45.7	4.0	OAO
6552.26042	− 15.2	4.1	OAO
6617.07400	− 22.2	3.7	OAO
6666.87938	5.8	4.6	OAO
6232.11546	− 38.1	5.3	Xinglong
6232.13878	− 28.3	5.1	Xinglong
6286.95306	− 13.5	8.1	Xinglong
6286.97627	− 16.9	7.9	Xinglong
6287.00037	− 20.3	7.4	Xinglong
6287.02420	− 23.6	7.7	Xinglong
6317.94617	10.1	7.8	Xinglong
6317.96965	3.4	7.6	Xinglong
6317.99284	2.8	7.9	Xinglong
6318.01605	4.8	8.6	Xinglong
6581.18750	6.8	8.3	Xinglong
6581.21073	− 3.7	6.7	Xinglong
6581.23392	− 4.8	8.0	Xinglong
6581.25725	− 10.9	8.2	Xinglong
6611.11370	14.2	6.9	Xinglong
6611.13689	21.9	7.4	Xinglong
6611.16007	34.2	7.4	Xinglong
6611.18325	39.9	6.4	Xinglong
6646.03568	8.9	12.1	Xinglong
6646.05898	10.6	11.6	Xinglong
6646.08226	7.1	13.3	Xinglong
6646.10544	5.4	12.5	Xinglong
4364.95416	44.2	4.8	Subaru
4470.70735	− 5.2	4.1	Subaru
4698.90077	46.0	5.0	Subaru

Downloaded from http://pasj.oxfordjournals.org/ at National Astronomical Observatory on January 3, 2015

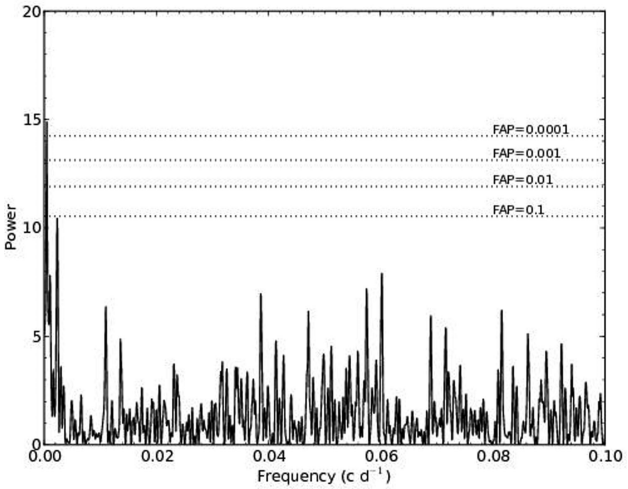

Fig. 3. Generalized Lomb–Scargle periodogram of the radial velocities of HD 14067. The normalization and *FAP* were calculated based on Horne and Baliunas (1986). There is a significant peak at $f \sim 4.9 \times 10^{-4}$ c d^{-1}, with $FAP < 1 \times 10^{-6}$. The dashed horizontal lines indicate FAP levels of 10^{-1}, 10^{-2}, 10^{-3}, and 10^{-4}, respectively, from bottom to top.

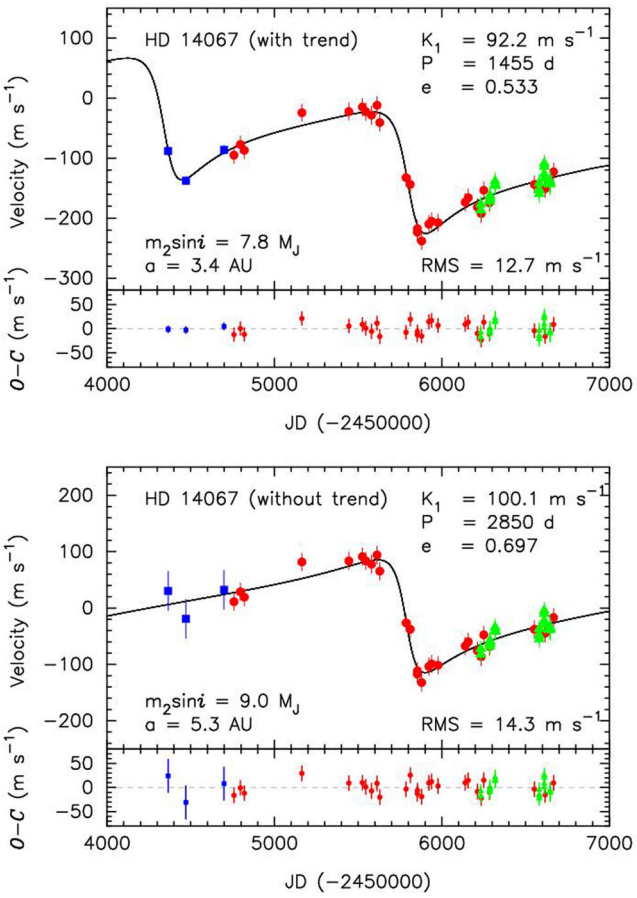

Fig. 4. Radial velocities of HD 14067 observed at OAO (red circles), Xinglong (green triangles), and Subaru (blue squares). The error bar for each point includes stellar jitter. The Keplerian orbits with (top panel) and without (bottom panel) a linear velocity trend are shown by the solid lines. Residuals to the orbital fitting are also shown in each panel. The rms values are 12.7 m s^{-1} (with linear trend) and 14.3 m s^{-1} (without linear trend), respectively. (Color online)

near the frequency of 4.9×10^{-4} c d^{-1} (figure 3). We also noticed that the star seems to exhibit a decreasing linear velocity trend besides the periodic variability. The significance of the trend depends on how large a systematic error is included in the first three Subaru data points, but such an error is difficult to estimate. Therefore, we performed the least-squares orbital fit by a single Keplerian with and without a linear trend, simultaneously. The orbital parameters and the uncertainties were derived using the Bayesian Markov chain Monte Carlo (MCMC) method (e.g., Ford 2005; Gregory 2005; Ford & Gregory 2007), following the analysis in Sato et al. (2013a). We took account of the velocity offsets of Xinglong and Subaru data relative to OAO data, $\Delta RV_{Xinglong-OAO}$ and $\Delta RV_{Subaru-OAO}$, as free parameters in the orbital fitting. Extra Gaussian noises of the three individual data sets, s_{OAO}, $s_{Xinglong}$, and s_{Subaru}, including intrinsic stellar jitters as well as unknown noise sources, were also incorporated as free parameters. We generated five independent chains having 10^7 points with an acceptance rate of about 25%, the first 10% of which were discarded, and confirmed that each parameter sufficiently converged based on the Gelman–Rubin statistic (Gelman & Rubin 1992). We derived the median value of the merged posterior probability distribution function (PDF) for each parameter and set the 1 σ uncertainty as a range of 15.87% to 84.13% of the PDF.

In figure 4 we plot the best-fitting Keplerian orbit with a linear velocity trend, together with the measured data points and their uncertainties obtained with the three different telescopes. The Keplerian orbit with a linear trend has parameters of period $P = 1455^{+13}_{-12}$ d, velocity semiamplitude $K_1 = 92.2^{+4.8}_{-4.7}$ m s^{-1}, eccentricity $e = 0.533^{+0.043}_{-0.047}$, and linear velocity trend $\dot{\gamma} = -22.4 \pm 2.2$ m s^{-1} yr^{-1}. Adopting the stellar mass of $M_\star = 2.4 \pm 0.2\ M_\odot$ given in table 1, we obtain $m_2 \sin i = 7.8 \pm 0.7\ M_J$ and $a = 3.4 \pm 0.1$ au for the companion. The rms scatter of the residuals to the Keplerian fit is 12.7 m s^{-1}. The Keplerian orbit without linear trend yields the parameters of $P = 2850^{+430}_{-290}$ d, $K_1 = 100.1^{+4.9}_{-4.8}$ m s^{-1}, and $e = 0.697^{+0.045}_{-0.051}$, and the corresponding parameters of the companion are $m_2 \sin i = 9.0 \pm 0.9\ M_J$ and $a = 5.3^{+0.6}_{-0.4}$ au. The rms scatter of the residuals of this model is 14.3 m s^{-1}, and these solutions are also shown in figure 4. The orbital parameters are summarized in table 3. Since the rms scatters of residuals in the two models are close to each other and both are comparable to the radial velocity jitter (~ 8 m s^{-1}) due to the stellar oscillations estimated by using the scaling relations of Kjeldsen and Bedding (1995), it is difficult to determine whether the linear velocity

Downloaded from http://pasj.oxfordjournals.org/ at National Astronomical Observatory on January 3, 2015

Table 3. Orbital parameters of HD 14067 b.

Parameter	HD 14067 b	
	with trend	without trend
P (d)	1455^{+13}_{-12}	2850^{+430}_{-290}
K_1 (m s^{-1})	$92.2^{+4.8}_{-4.7}$	$100.1^{+4.9}_{-4.8}$
e	$0.533^{+0.043}_{-0.047}$	$0.697^{+0.045}_{-0.051}$
ω (°)	$109.9^{+5.6}_{-5.7}$	$102.1^{+5.1}_{-5.3}$
T_p (JD−2450000)	1443^{+31}_{-37}	92^{+586}_{-862}
s_{OAO} (m s^{-1})	$13.8^{+2.6}_{-2.0}$	$14.9^{+2.7}_{-2.1}$
$s_{Xinglong}$ (m s^{-1})	$12.2^{+3.0}_{-2.4}$	$12.3^{+3.0}_{-2.4}$
s_{Subaru} (m s^{-1})	$5.4^{+22.2}_{-4.6}$	34^{+31}_{-14}
$\Delta RV_{Xinglong-OAO}$ (m s^{-1})	$19.8^{+6.0}_{-6.0}$	$21.5^{+6.1}_{-6.2}$
$\Delta RV_{Subaru-OAO}$ (m s^{-1})	$3.6^{+11.3}_{-12.5}$	$-8.7^{+24.1}_{-24.2}$
$\dot{\gamma}$ (m s^{-1} yr^{-1})	$-22.4^{+2.2}_{-2.2}$	—
$a_1 \sin i$ (10^{-3} au)	$10.43^{+0.50}_{-0.51}$	$18.9^{+1.8}_{-1.4}$
$f_1(m)$ (10^{-7} $M_\odot$)	$0.714^{+0.099}_{-0.91}$	$1.10^{+0.16}_{-0.15}$
$m_2 \sin i$ (M_J)	7.8 ± 0.7	9.0 ± 0.9
a (au)	3.4 ± 0.1	$5.3^{+0.6}_{-0.4}$
N_{OAO}	27	
$N_{Xinglong}$	22	
N_{Subaru}	3	
rms (m s^{-1})	12.7	14.3
BIC	447.07	458.24

trend should be included. We calculated the Bayesian information criterion ($BIC = -2 \ln \mathcal{L}_{max} + k \ln N$: Schwarz 1978; Liddle 2004, 2007) of the two models, where $\mathcal{L}_{max}$ is the maximum likelihood of each model, k denotes the number of free parameters in a model, and N is the number of data points. The Keplerian orbit with a linear velocity trend has a smaller BIC value than the model without trend, but the former solution is largely constrained by only having three measurements with Subaru, and hence severely affected by the velocity difference between data sets with different instruments. The velocity trend corresponds to a possible outer companion with

$$\frac{m_c \sin i_c}{a_c^2} \sim \frac{\dot{\gamma}}{G} = (0.13 \pm 0.01)\, M_J\ \mathrm{au}^{-2}, \quad (1)$$

by using the order-of-magnitude relation of Winn et al. (2009), where m_c, i_c, and a_c are the mass, orbital inclination, and semi major axis of the companion, respectively. This means that if the companion lies outside ∼10 au, it will not be an exoplanet with $m_c < M_b$, where $M_b \simeq 13\, M_J$ is the lower mass limit of a typical brown dwarf. On the other hand, there is no evidence to show that HD 14067 has any companion star so far. After removal of the orbital fitting, there is no significant peak with $FAP < 0.1$ on the generalized Lomb–Scargle periodograms of the velocity residuals (figure 5).

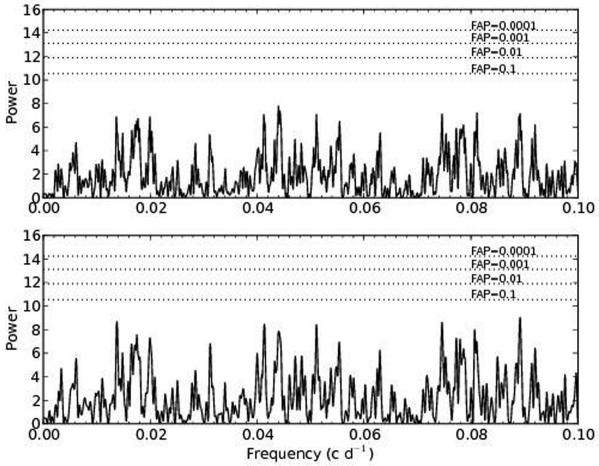

Fig. 5. Generalized Lomb–Scargle periodograms of the radial velocity residuals after Keplerian orbital fitting with (upper panel) and without (lower panel) a linear trend. Neither of them shows any significant peak with FAP below 0.1.

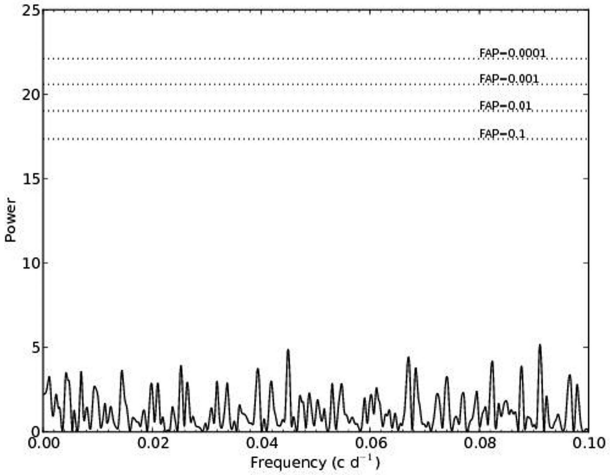

Fig. 6. Generalized Lomb–Scargle periodogram of the Hipparcos photometric data of HD 14067. The dashed horizontal lines indicate *FAP* levels of 10^{-1}, 10^{-2}, 10^{-3}, and 10^{-4}, respectively, from bottom to top.

The Hipparcos satellite made a total number of 86 photometric observations for HD 14067 during the period from 1990 January to 1993 February. The scatter of Hipparcos magnitude (H_p) came down to 0.007 mag, but the photometry was not contemporaneous with the radial velocity measurements and also the time span (∼1100 d) was not long enough to cover a whole radial velocity period. Figure 6 shows the generalized Lomb–Scargle periodogram of the HD 14067 photometric data. We did not find any clue that the radial velocity variation correlates with brightness changes due to stellar spots.

Downloaded from http://pasj.oxfordjournals.org/ at National Astronomical Observatory on January 3, 2015

We also performed spectral line shape analysis for the star following the method in Sato et al. (2007). Cross-correlation profiles of the two stellar templates, which were extracted from five I_2-superposed spectra at phases of velocity maximum (JD∼2455600) and velocity minimum (JD∼2455900) by using the technique of Sato et al. (2002), were derived for about 90 spectral segments (4–5 Å width each). Then three bisector quantities of the cross-correlation profiles, BVS, BVC, and BVD, were calculated, and they are the velocity difference between the two flux levels of the bisector, the difference of the BVS of the upper and lower halves of the bisector, and the average of the bisector at three flux levels, respectively. We used the flux levels of 25%, 50%, and 75% of each cross-correlation profile to calculate the above three bisector quantities. As a result, we obtained $BVS = -8.4 \pm 3.8\,\mathrm{m\,s^{-1}}$, $BVC = 2.7 \pm 1.8\,\mathrm{m\,s^{-1}}$, and $BVD = -186.7 \pm 7.1\,\mathrm{m\,s^{-1}}$ ($\simeq 2K_1$), suggesting that the observed radial velocity variations are not caused by distortion of the spectral lines but by parallel shifts of them as expected in the case of orbital motion.

5 Conclusion

We report on the detection of a long-period substellar companion to the G9 III evolved intermediate-mass ($M_\star = 2.4\,M_\odot$) star HD 14067 from the Subaru and Japan–China planet search program. The radial velocity variation of the star can be well explained by the gravitational perturbation of an unseen surrounding companion. The orbit can be well fitted with two models—Keplerian orbits with and without a linear velocity trend, both of which have similar velocity residuals, while the former model has a smaller BIC value than the latter one. The minimum mass of the companion is $m_2 \sin i = 7.8 \pm 0.7\,M_\mathrm{J}$ (with velocity trend) or $m_2 \sin i = 9.0 \pm 0.9\,M_\mathrm{J}$ (without trend), suggesting a long-period giant planet orbiting an evolved giant star. It is notable that HD 14067 b is among the planets with the largest semimajor axes and orbital periods around evolved intermediate-mass stars. The possible decreasing linear velocity trend ($-22.4\,\mathrm{m\,s^{-1}\,yr^{-1}}$) may suggest an additional outer companion around this star. Unfortunately, the time span of observations is not long enough either to distinguish between these two possible orbital solutions or to confirm the existence of this outer companion. Therefore, continued radial velocity observations are essential to characterizing the orbital properties of this system.

Although the fitting of a Keplerian orbit with a linear trend significantly reduces the resulting eccentricity, orbital solutions for both models show that the eccentricity of HD 14067 b is large ($e = 0.533$ with a velocity trend, or $e = 0.697$ without velocity trend), making this planet one of the most eccentric planet ever discovered around stars

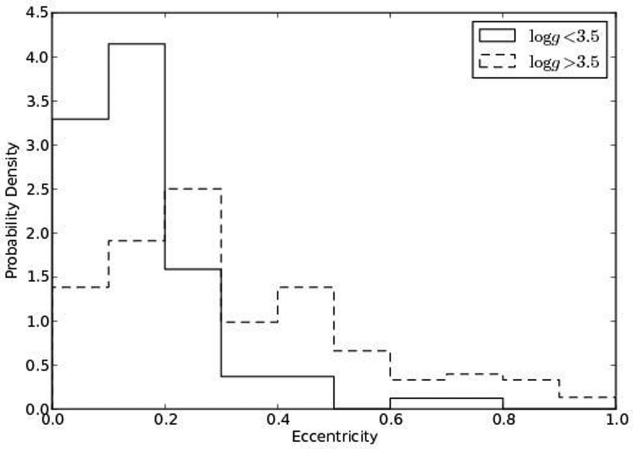

Fig. 7. Probability density distribution of eccentricities of radial velocity planets with 0.5 au $< a <$ 3.0 au around main sequence stars (log $g_\star > 3.5$) and around evolved stars (log $g_\star < 3.5$) are plotted by dashed lines and solid lines, respectively.

with $M_\star > 1.5\,M_\odot$. Figure 7 shows a concentration toward low eccentricity for planets around off-main-sequence stars (log $g_\star < 3.5$), while the eccentricity distribution of planets around main sequence stars reaches its peak at $e = 0.2-0.3$. To avoid bias due to the lack of short-period, circularized planets around evolved stars, only planets with a semimajor axis of 0.5 au $< a <$ 3.0 au are plotted.

The high eccentricity of HD 14067 b might originate from (a) the incomplete circularization due to its large distance to its host, because $|\dot{e}|$ decreases as a^{-8} (Zahn 1989), or (b) the perturbation of an outer companion. We plot the eccentricities against the semimajor axes of exoplanets found around evolved and main sequence stars by using the Doppler technique in figure 8, where the colors are coded with different ranges of stellar mass. It is clearly shown that almost all planets orbiting high-mass ($M_\star > 2.0\,M_\odot$) stars have periastron distances $q = a(1-e) > 0.66$ au. The closest blue point to HD 14067 b in figure 8 is HD 120084 b, which also has an eccentric orbit ($a = 4.3$ au, $e = 0.66$, see Sato et al. 2013a) around an evolved star with $M_\star = 2.39\,M_\odot$. The large semimajor axes of these two long-period planets support the former possibility of the origin of the large eccentricities, which means they were less affected by the orbital circularization during the RGB phase compared with other planets around evolved stars.

We also noticed that most planet-harboring evolved stars accompanied by eccentric planets ($e > 0.4$) also exhibit linear radial velocity trends besides the periodic variations caused by their companions, or lie in systems with more than two objects. For example, HD 1690 (with an eccentric planet of $e = 0.64 \pm 0.04$) shows a linear decreasing velocity trend of $\dot{\gamma} = -7.2 \pm 0.4\,\mathrm{m\,s^{-1}}$ (Moutou et al. 2011). HD 102272 c ($e = 0.68 \pm 0.06$) is the

Downloaded from http://pasj.oxfordjournals.org/ at National Astronomical Observatory on January 3, 2015

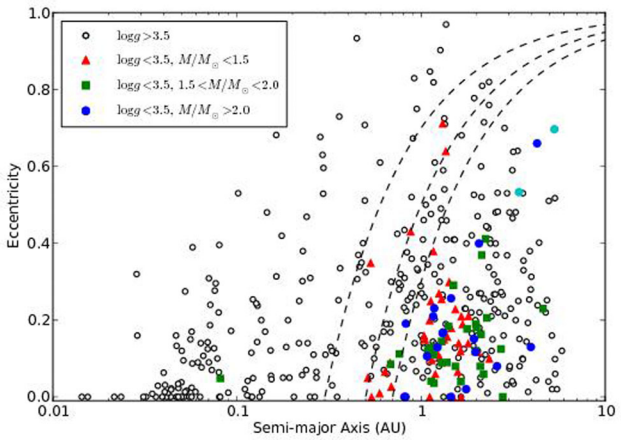

Fig. 8. Eccentricities versus semimajor axes of exoplanets discovered by the radial velocity technique. Planets around low-mass ($M_* < 1.5\ M_\odot$), intermediate-mass ($1.5\ M_\odot < M_* < 2.0\ M_\odot$), and high-mass ($M_* > 2.0\ M_\odot$) evolved stars with $\log g_* < 3.5$ are plotted by red filled triangles, green filled squares, and blue filled circles, respectively. The two possible solutions of the newly detected companion HD 14067 b are plotted by the cyan circles. Planets around stars with $\log g_* > 3.5$ are plotted by open circles. Dashed lines indicate periastron distances [$q = a(1 - e)$] of 0.3, 0.5, and 0.7 au, respectively, from left to right. (Color online)

outer companion of a double-planet system (Niedzielski et al. 2009). And the parent stars of HD 137759 b ($e = 0.70 \pm 0.01$, Frink et al. 2002) and HD 110014 b ($e = 0.462 \pm 0.069$, de Medeiros et al. 2009) are both members of double star systems. These facts imply that the high eccentricities of such planets can be excited by the gravitational perturbations of additional objects, or the existences of these objects stop the orbital circularizations of the planets. If the relatively small eccentricities of planets around evolved stars are caused by the tidal circularization when the parent stars expand during the RGB phase, it is expected to see higher orbital eccentricities with an increasing semimajor axis, especially in systems where a distant outer perturbator exists. Future discoveries with longer observational baselines will be of much help for a solution to this crucial question.

Acknowledgments

This research is based on data collected at the Subaru Telescope and Okayama Astrophysical Observatory (OAO), both operated by National Astronomical Observatory of Japan (NAOJ), and the 2.16 m telescope at Xinglong Observatory, operated by National Astronomical Observatories, Chinese Academy of Sciences. We are grateful to all the staff members of Subaru, OAO, and Xinglong for their support during the observations. We thank students of Tokyo Institute of Technology and Kobe University for their kind help for the observations at Subaru and OAO. LW is supported by the Young Researcher Grant of National Astronomical Observatories, Chinese Academy of Sciences. BS was partly supported by MEXT's program "Promotion of Environmental Improvement for Independence of Young Researchers" under the Special Coordination Funds for Promoting Science and Technology and by a Grant-in-Aid for Young Scientists (B) 20740101 from Japan Society for the Promotion of Science (JSPS). BS is supported by a Grant-In-Aid for Scientific Research (C) 23540263 from JSPS and HI is supported by a Grant-In-Aid for Scientific Research (A) 23244038 from JSPS. YJL and LW are supported by the National Natural Science Foundation of China under grants 11173031. This research has made use of the SIMBAD database, operated at CDS, Strasbourg, France.

References

Alonso, A., Arribas, S., & Martínez-Roger, C. 1999, A&AS, 140, 261
Alonso, A., Arribas, S., & Martínez-Roger, C. 2001, A&A, 376, 1039
Brucalassi, A., et al. 2014, A&A, 561, L9
Castelli, F., & Kurucz, R. L. 2004, astro-ph/0405087
Collier Cameron, A., et al. 2010, MNRAS, 407, 507
Currie, T. 2009, ApJ, 694, L171
da Silva, L., et al. 2006, A&A, 458, 609
de Medeiros, J. R., & Mayor, M. 1999, A&AS, 139, 433
de Medeiros, J. R., Setiawan, J., Hatzes, A. P., Pasquini, L., Girardi, L., Udry, S., Döllinger, M. P., & da Silva, L. 2009, A&A, 504, 617
Döllinger, M. P., Hatzes, A. P., Pasquini, L., Guenther, E. W., Hartmann, M., & Girardi, L. 2009, A&A, 499, 935
Ford, E. B. 2005, AJ, 129, 1706
Ford, E. B., & Gregory, P. C. 2007, in ASP Conf. Ser., 371, Statistical Challenges in Modern Astronomy IV, ed. G. J. Babu & E. D. Feigelson (San Francisco: ASP), 189
Ford, E. B., & Rasio, F. A. 2008, ApJ, 686, 621
Frink, S., Mitchell, D. S., Quirrenbach, A., Fischer, D. A., Marcy, G. W., & Butler, R. P. 2002, ApJ, 576, 478
Gelman, A., & Rubin, D. 1992, Statistical Science, 7, 457
Gettel, S., Wolszczan, A., Niedzielski, A., Nowak, G., Adamów, M., Zieliński, P., & Maciejewski, G. 2012, ApJ, 745, 28
Gregory, P. C. 2005, ApJ, 631, 1198
Hatzes, A. P., Guenther, E. W., Endl, M., Cochran, W. D., Döllinger, M. P., & Bedalov, A. 2005, A&A, 437, 743
Hekker, S., & Meléndez, J. 2007, A&A, 475, 1003
Horne, J. H., & Baliunas, S. L. 1986, ApJ, 302, 757
Izumiura, H. 1999, Publ. Yunnan Obs., 77
Izumiura, H. 2005, J. Korean Astron. Soc., 38, 81
Johnson, J. A., et al. 2007, ApJ, 665, 785
Johnson, J. A., et al. 2010, ApJ, 721, L153
Johnson, J. A., et al. 2011, ApJS, 197, 26
Jones, M. I., Jenkins, J. S., Bluhm, P., Rojo, P., & Melo, C. H. F. 2014, A&A, 566, A113
Jones, M. I., Jenkins, J. S., Rojo, P., Melo, C. H. F., & Bluhm, P. 2013, A&A, 556, A78
Kambe, E., et al. 2002, PASJ, 54, 865
Kjeldsen, H., & Bedding, T. R. 1995, A&A, 293, 87
Kretke, K. A., Lin, D. N. C., Garaud, P., & Turner, N. J. 2009, ApJ, 690, 407
Lee, B.-C., Han, I., & Park, M.-G. 2013, A&A, 549, A2
Lejeune, T., & Schaerer, D. 2001, A&A, 366, 538
Liddle, A. R. 2004, MNRAS, 351, L49
Liddle, A. R. 2007, MNRAS, 377, L74

Downloaded from http://pasj.oxfordjournals.org/ at National Astronomical Observatory on January 3, 2015

Liu, Y.-J., Sato, B., Zhao, G., & Ando, H. 2009, Res. Astron. Astrophys., 9, 1
Liu, Y. J., Tan, K. F., Wang, L., Zhao, G., Sato, B., Takeda, Y., & Li, H. N. 2014, ApJ, 785, 94
Lovis, C., & Mayor, M. 2007, A&A, 472, 657
Moutou, C., et al. 2011, A&A, 527, A63
Niedzielski, A., Goździewski, K., Wolszczan, A., Konacki, M., Nowak, G., & Zieliński, P. 2009, ApJ, 693, 276
Noguchi, K., et al. 2002, PASJ, 54, 855
Nordhaus, J., Spiegel, D. S., Ibgui, L., Goodman, J., & Burrows, A. 2010, MNRAS, 408, 631
Omiya, M., et al. 2009, PASJ, 61, 825
Omiya, M., et al. 2012, PASJ, 64, 34
Perryman, M. A. C., et al. 1997, A&A, 323, L49
Sato, B., Kambe, E., Takeda, Y., Izumiura, H., & Ando, H. 2002, PASJ, 54, 873
Sato, B., et al. 2003, ApJ, 597, L157
Sato, B., et al. 2007, ApJ, 661, 527
Sato, B., et al. 2008a, PASJ, 60, 539
Sato, B., et al. 2008b, PASJ, 60, 1317
Sato, B., et al. 2010, PASJ, 62, 1063
Sato, B., et al. 2012, PASJ, 64, 135
Sato, B., et al. 2013a, PASJ, 65, 85
Sato, B., et al. 2013b, ApJ, 762, 9
Schlegel, D. J., Finkbeiner, D. P., & Davis, M. 1998, ApJ, 500, 525
Schwarz, G. 1978, Ann. Statistics, 6, 461
Setiawan, J., et al. 2003, A&A, 398, L19
Szabó, G. M., et al. 2011, ApJ, 736, L4
Takeda, G., & Rasio, F. A. 2005, ApJ, 627, 1001
van Leeuwen, F. 2007, A&A, 474, 653
Wang, L., et al. 2012, Res. Astron. Astrophys., 12, 84
Winn, J. N., Johnson, J. A., Albrecht, S., Howard, A. W., Marcy, G. W., Crossfield, I. J., & Holman, M. J. 2009, ApJ, 703, L99
Wittenmyer, R. A., Endl, M., Wang, L., Johnson, J. A. W., Tinney, C. G., & O'Toole, S. J. 2011, ApJ, 743, 184
Zahn, J.-P. 1989, A&A, 220, 112
Zechmeister, M., & Kürster, M. 2009, A&A, 496, 577
Zhao, G., & Li, H.-B. 2001, Chin. J. Astron. Astrophys., 1, 555

Downloaded from http://pasj.oxfordjournals.org/ at National Astronomical Observatory on January 3, 2015